CREBH normalizes dyslipidemia and halts atherosclerosis in diabetes by decreasing circulating remnant lipoproteins

Masami Shimizu-Albergine,[1] Debapriya Basu,[2] Jenny E. Kanter,[1] Farah Kramer,[1] Vishal Kothari,[1] Shelley Barnhart,[1] Carissa Thornock,[1] Adam E. Mullick,[3] Noemie Clouet-Foraison,[1] Tomas Vaisar,[1] Jay W. Heinecke,[1] Robert A. Hegele,[4,5,6] Ira J. Goldberg,[2] and Karin E. Bornfeldt[1,7]

[1]Department of Medicine, Division of Metabolism, Endocrinology and Nutrition, University of Washington Medicine Diabetes Institute, University of Washington, Seattle, Washington, USA. [2]Division of Endocrinology, Diabetes and Metabolism, Department of Medicine, New York University Grossman School of Medicine, New York, New York, USA. [3]Ionis Pharmaceuticals, Carlsbad, California, USA. [4]Robarts Research Institute, [5]Department of Biochemistry, and [6]Department of Medicine, Western University, London, Ontario, Canada. [7]Department of Laboratory Medicine and Pathology, University of Washington Medicine Diabetes Institute, University of Washington, Seattle, Washington, USA.

Loss-of-function mutations in the transcription factor *CREB3L3* (CREBH) associate with severe hypertriglyceridemia in humans. CREBH is believed to lower plasma triglycerides by augmenting the activity of lipoprotein lipase (LPL). However, by using a mouse model of type 1 diabetes mellitus (T1DM), we found that greater liver expression of active CREBH normalized both elevated plasma triglycerides and cholesterol. Residual triglyceride-rich lipoprotein (TRL) remnants were enriched in apolipoprotein E (APOE) and impoverished in APOC3, an apolipoprotein composition indicative of increased hepatic clearance. The underlying mechanism was independent of LPL, as CREBH reduced both triglycerides and cholesterol in LPL-deficient mice. Instead, APOE was critical for CREBH's ability to lower circulating remnant lipoproteins because it failed to reduce TRL cholesterol in *Apoe*$^{-/-}$ mice. Importantly, individuals with *CREB3L3* loss-of-function mutations exhibited increased levels of remnant lipoproteins that were deprived of APOE. Recent evidence suggests that impaired clearance of TRL remnants promotes cardiovascular disease in patients with T1DM. Consistently, we found that hepatic expression of CREBH prevented the progression of diabetes-accelerated atherosclerosis. Our results support the proposal that CREBH acts through an APOE-dependent pathway to increase hepatic clearance of remnant lipoproteins. They also implicate elevated levels of remnants in the pathogenesis of atherosclerosis in T1DM.

Introduction

The basic leucine zipper transcription factor CREBH (gene name *CREB3L3*; cAMP responsive element–binding protein 3–like 3) was identified 20 years ago (1), and was found to be expressed primarily in the liver, with more limited expression in the intestine (1, 2). Importantly, individuals with heterozygous *CREB3L3* loss-of-function or missense mutations exhibit hypertriglyceridemia (3, 4). Furthermore, a recent study found that individuals with severe hypertriglyceridemia were 20 times more likely than controls to carry loss-of-function mutations in *CREB3L3* (5). Because *CREB3L3* loss-of-function mutations are rare, it is not yet known if such individuals exhibit an increased cardiovascular disease risk.

▶ **Related Commentary: https://doi.org/10.1172/JCI154677**

Conflict of interest: AEM is employed by Ionis Pharmaceuticals. KEB and JEK have received research support from Novo Nordisk A/S.

Submitted: July 19, 2021; **Accepted:** September 1, 2021; **Published:** November 15, 2021.
Reference information: *J Clin Invest*. 2021;131(22):e153285.
https://doi.org/10.1172/JCI153285.

CREBH is an important inducer of specific gene sets involved in both lipid and glucose metabolism (2, 4, 6–12). Its marked effects on plasma triglyceride (TG) levels have been ascribed to induction of its target genes, *APOC2* and *APOA5*. The products of these genes aid in the activation of lipoprotein lipase (LPL), and are required for effective lipolysis of TG-rich lipoproteins (TRLs) and conversion of those particles to remnant lipoproteins and their removal by the liver (2, 13). TRLs encompass chylomicrons containing APOB48 that are derived from the intestine after a meal and very-low-density lipoproteins (VLDLs) containing APOB100 that are derived from the liver between meals.

Remnant lipoproteins arise when the TG cargo of precursor TRLs (chylomicrons and VLDLs) is hydrolyzed by LPL tethered along capillaries by glycosylphosphatidylinositol-anchored HDL-binding protein 1 (GPIHBP1) (14), primarily in adipose tissue, skeletal muscle, and heart. As the lipoprotein particles gradually become smaller and less enriched in TGs versus cholesterol during this lipolytic process, they also become enriched in APOE and impoverished in APOCs as compared with their parent TRLs (15). Thus, they fit the definition of remnants. (There is no universally agreed upon method for quantifying remnants, however; see ref. 16). The remnants are then either converted to LDL (in

the case of some APOB100-containing VLDL remnants, often referred to as intermediate-density lipoprotein; IDL) or cleared by the liver by APOE-dependent uptake primarily through the LDL receptor (LDLR) and LDL receptor–related protein 1 (LRP1).

Remnant lipoproteins are highly atherogenic, as evidenced by the increased cardiovascular disease (CVD) risk in individuals with remnant removal disease (also known as familial dysbetalipoproteinemia or type III hyperlipoproteinemia; refs. 16–19). This condition is usually caused by homozygosity of the APOE2 isoform, which has low affinity for the LDL family receptors. Remnant removal disease associates with reduced hepatic clearance of remnant lipoproteins when another primary or secondary lipid abnormality is also present. Conversely, very large TRLs (chylomicrons and large VLDL) are much less atherogenic (20), likely because these particles are too large to effectively enter the artery wall (13).

Recent evidence supports the proposal that impaired clearance of remnant lipoproteins also contributes to the increased CVD risk associated with diabetes. In particular, we recently demonstrated that elevated serum levels of APOC3, which slows clearance of TRLs and their remnants, predict incident coronary artery disease in people with type 1 diabetes mellitus (T1DM) (21). These results were confirmed in an independent T1DM cohort (22). Serum levels of APOC3 also associated positively with the presence of coronary artery calcium, a measure of atherosclerosis in these T1DM patients (23). Furthermore, silencing APOC3 halted atherosclerosis in our mouse model of T1DM (21). Concomitantly, silencing APOC3 prevented the accumulation of APOB and APOE in the artery wall, suggesting reduced remnant accumulation. Together, these observations indirectly support the involvement of remnants in the CVD that associates with diabetes.

APOC3 slows the clearance of TRLs by 2 mechanisms. First, it inhibits LPL activity — perhaps by preventing the LPL that is tethered to the microvascular endothelium from accessing the TGs in these particles — thereby reducing TG hydrolysis and conversion of chylomicrons to chylomicron remnants and VLDL to IDL and further to LDL (24, 25). Because lipolyzed TRL–derived particles are cleared more effectively by the liver than nascent TRLs (26, 27), inhibition of lipolysis results in impaired clearance of TRLs and TRL remnants. Second, APOC3 interferes with hepatic uptake of APOE-rich remnants by LDLR and LRP1 (28–30). Thus, APOC3 silencing results in a reduction in TG and cholesterol levels also in the absence of LPL (28).

To determine whether activation of hepatic CREBH exerts protective effects on TRLs, remnant accumulation, and atherosclerosis in the setting of diabetes, we used a liver-targeted adeno-associated virus (AAV) to introduce the active N-terminal portion of mouse CREBH into our T1DM mouse model of diabetes-accelerated atherosclerosis. After investigating the mechanism of CREBH's protective effects, we performed targeted proteomic analysis of VLDL and IDL from individuals with rare *CREB3L3* loss-of-function mutations. The studies uncovered a hitherto unknown LPL-independent effect of CREBH: improved hepatic clearance of remnant lipoproteins through an APOE-dependent pathway that halts the progression of diabetes-accelerated atherosclerosis.

Results

Liver-specific expression of active CREBH induces hepatic expression of genes involved in clearance of remnant lipoproteins. CREBH is located in the endoplasmic reticulum (ER) as an inactive full-length form. Upon an ER stress response, CREBH is transported to the Golgi, where it is cleaved by site-1 and site-2 proteases, liberating its N-terminal portion. This fragment is then transferred to the nucleus to induce the expression of its target genes (31). The mechanism of CREBH activation is therefore similar to that of sterol regulatory element–binding proteins (SREBPs) and ATF6. Because full-length CREBH competes with SREBPs for cleavage by the site-1 and site-2 proteases, and therefore inhibits the activation of SREBPs (32), we elected to express the N-terminal active form of CREBH under control of a liver-selective promoter using an AAV approach. When we validated the strategy in *Ldlr*$^{-/-}$ mice fed a high-fat/high-sucrose diet, a model of prediabetes (Supplemental Figures 1–3; supplemental material available online with this article; https://doi.org/10.1172/JCI153285DS1), we obtained results similar to those of previous studies on CREBH (32, 33): increased expression of CREBH target genes, improved glucose tolerance, lipid lowering, and prevention of atherosclerosis. Expression of the active N-terminal CREBH did not alter endogenous *Creb3l3* mRNA expression (Supplemental Figure 1).

We then applied this approach to our mouse model of T1DM-accelerated atherosclerosis (21, 34). As our previous data showed that diabetes promotes the progression of preexisting atherosclerotic lesions through an APOC3-dependent mechanism (21), we used a similar experimental design (Figure 1A). Male *Ldlr*$^{-/-}$ mice were fed a high-fat, semipurified diet (34) for 16 weeks to allow advanced lesions to develop. The mice were then injected i.v. with control empty AAV (cAAV-DJ/8) or CREBH AAV-DJ/8 targeted to the liver by the thyroxine-binding globulin (TBG) promoter (ref. 35; 5×10^{10} genome copies [GC] per mouse). One week later, the mice were injected with lymphocytic choriomeningitis virus (LCMV) to induce diabetes or with saline for nondiabetic littermate controls (at a time point defined as baseline), and were then fed a low-fat, semipurified diet for another 6 weeks. This diet prevents the extreme hyperlipidemia associated with diabetes in mice fed high-fat diets (34). Diabetic mice received exogenous insulin to prevent excessive weight loss and ketonuria.

At the end of the study, we first analyzed liver and intestine mRNA levels to verify that CREBH expression was liver specific and that CREBH target genes were induced in both the nondiabetic and diabetic mice. We detected AAV-derived *Creb3l3* mRNA in the liver of the nondiabetic and diabetic mice injected with CREBH AAV but not in those injected with cAAV (Figure 1B). The injections did not affect endogenous *Creb3l3* mRNA levels (Supplemental Figure 4A). CREBH AAV increased known CREBH target genes (2, 36, 37), including *Apoc2*, *Apoa5*, *Apoa4*, *Cidec*, and *Fgf21* in both the nondiabetic and diabetic mice (Figure 1B). It did not affect the elevated *Apoc3* mRNA levels in the diabetic mice, suggesting that *Apoc3* is not one of its targets, consistent with previous studies (2, 33), and it did not alter hepatic TG levels (Figure 1, B and C). Expression of active CREBH modestly increased *Apob* mRNA levels without affecting hepatic APOB100 and APOB48 protein levels (diabetes had no effect), and neither

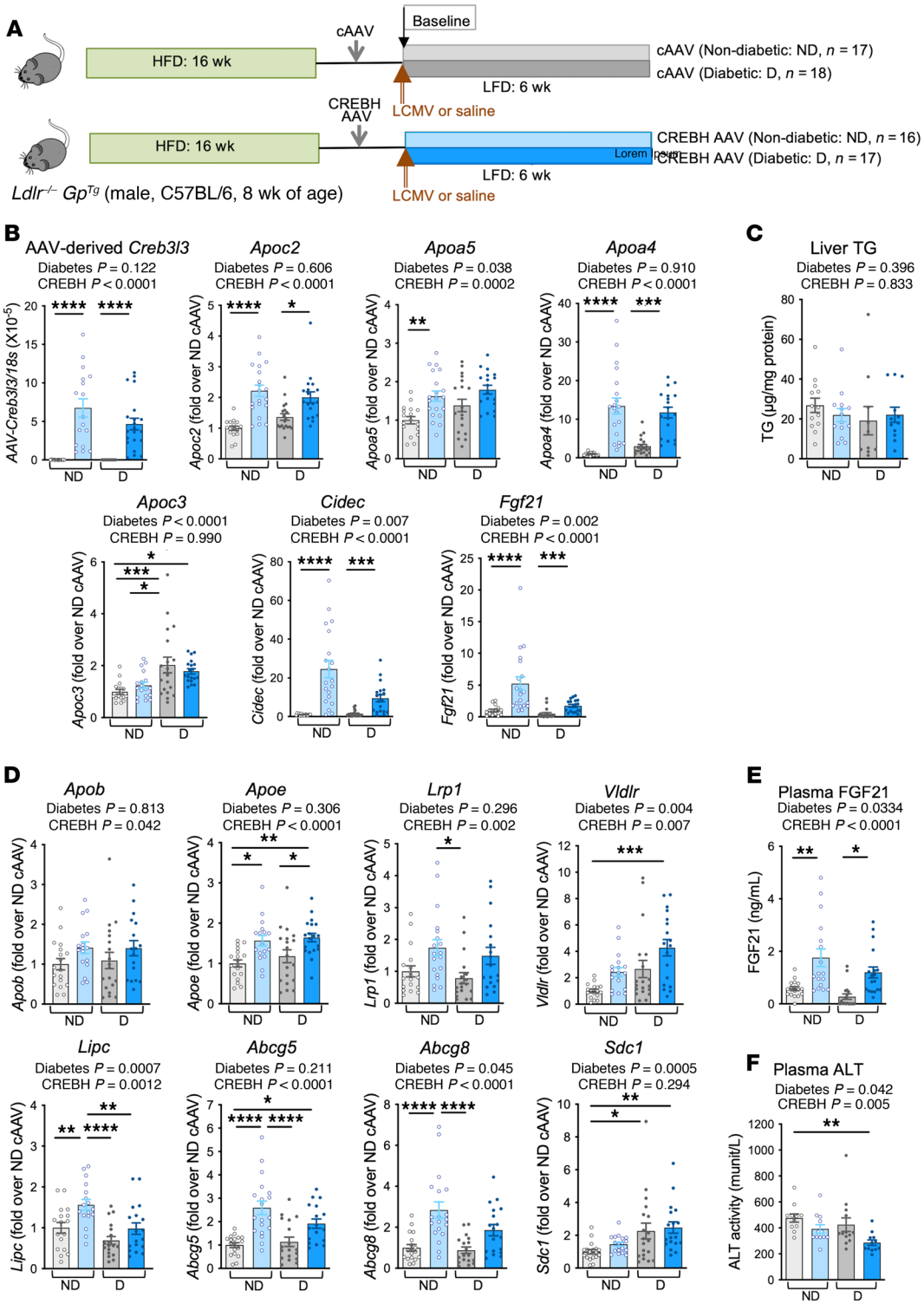

Figure 1. Liver-specific expression of active CREBH induces hepatic expression of genes involved in hepatic clearance of remnant lipoproteins. (**A**) Male *Ldlr*$^{-/-}$ *Gp*^{Tg} mice were fed a high-fat diet (HFD) for 16 weeks, followed by a regular chow to normalize lipids for 1 week. Empty control TGB-AAV-DJ/8 (cAAV, 5×10^{10} GC) or TBG-AAV-DJ/8 containing the active form of mouse CREBH (CREBH AAV, 5×10^{10} GC) was then injected i.v. After 1 week, the mice were rendered diabetic using lymphocytic choriomeningitis virus (LCMV). Saline was used as control in nondiabetic littermates. At the time of LCMV injection, the mice were switched to a low-fat, semipurified diet (LFD) and maintained for an additional 4 weeks after the onset of diabetes. At the end of the study, the liver was collected for measurements of gene expression by real-time PCR (**B** and **D**) and liver TG content (**C**). Plasma was used for measurements of FGF21 (**E**) and alanine transaminase (ALT) to confirm lack of liver toxicity (**F**) by ELISA. ND, nondiabetic mice; D, diabetic mice. Mean ± SEM. *$P < 0.05$; **$P < 0.01$; ***$P < 0.001$; ****$P < 0.0001$ by 2-way ANOVA (overall effects shown above panels) followed by Tukey's multiple comparisons test (**B**, **D**, and **E**: $n = 17$ ND cAAV, $n = 16$ ND CREBH AAV, $n = 18$ D cAAV, $n = 17$ D CREBH AAV; **C** and **F**: $n = 13$ ND cAAV, $n = 14$ ND CREBH AAV, $n = 10$ D cAAV, $n = 12$ D CREBH AAV).

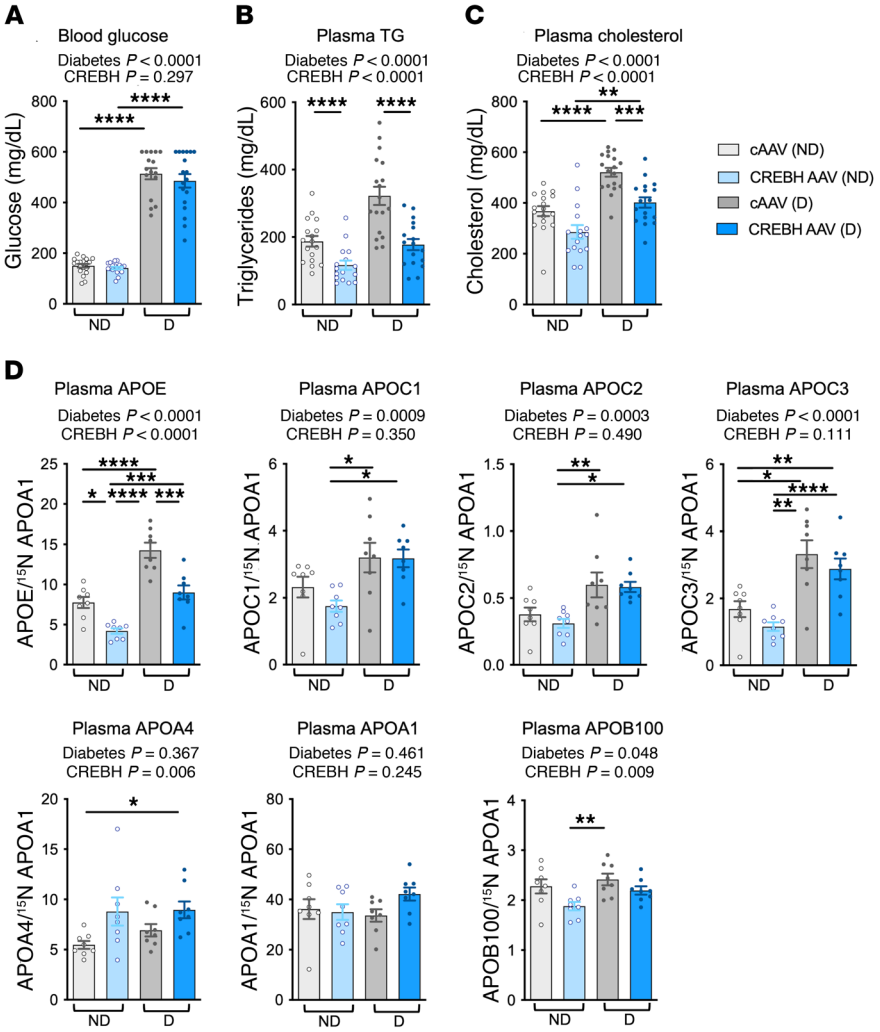

Figure 2. Hepatic expression of active CREBH reduces plasma lipids and APOE. Diabetic (D) and nondiabetic (ND) mice with hepatic expression of active CREBH were generated as described in the Figure 1 legend. (**A**) Blood glucose was measured 1 day before the mice were euthanized. Plasma collected at the end point was used for measurement of TG (**B**) and cholesterol (**C**) (n = 17 ND cAAV, n = 16 ND CREBH AAV, n = 18 D cAAV, n = 17 D CREBH AAV). (**D**) Plasma apolipoproteins were analyzed by targeted mass spectrometry and normalized to ^{15}N-APOA1 (n = 8/group). Mean ± SEM. *P < 0.05; **P < 0.01; ***P < 0.001; ****P < 0.0001 by 2-way ANOVA (overall effects shown above panels) followed by Tukey's multiple comparisons test.

CREBH nor diabetes altered *Mttp* or *Fasn* levels (Supplemental Figure 4, A and B), indicating that VLDL production and lipogenesis were largely unaffected by both CREBH and diabetes, as in previous studies (32, 38, 39).

Importantly, in addition to the LPL activators *Apoc2* and *Apoa5*, CREBH induced genes involved in hepatic clearance of remnant lipoproteins and sterols, including *Apoe*, *Lrp1*, *Vldlr*, *Lipc*, *Abcg5*, and *Abcg8* (Figure 1D). LRP1 and the VLDL receptor (*Vldlr*) mediate hepatic uptake of TRL remnants by binding to APOE on those particles (30, 40); hepatic lipase (*Lipc*) mediates the conversion of VLDL remnants to LDL and plays a role in remnant clearance (41); and the sterol transport proteins ABCG5 and ABCG8 mediate excretion of sterols into bile (42). Conversely, diabetes had no consistent effect on expression of these genes, but it increased the expression of *Sdc1* (syndecan 1), a proteoglycan that contributes to hepatic clearance of TRL lipoproteins (ref. 43 and Figure 1D).

Consistent with CREBH's ability to induce hepatic *Fgf21* expression, mice injected with CREBH AAV had higher levels of plasma FGF21 (Figure 1E). The mice expressing the active CREBH displayed no detectable hepatotoxicity (Figure 1F).

To investigate tissue specificity, we analyzed gene expression in the intestine, a second site of endogenous CREBH expression. The AAV-derived active CREBH was not expressed in the intestine, did not alter endogenous *Creb3l3* mRNA levels, and did not increase CREBH target genes such as *Apoa4* (Supplemental Figure 4C).

Together, these results demonstrate that hepatic CREBH activity induces genes involved in the clearance of TRL remnants in addition to its well-investigated target genes, such as *Apoc2* and *Apoa5*.

Hepatic CREBH activity normalizes elevated plasma APOE levels and alters APOE and APOC3 loading of TRLs and remnants in diabetic mice. In the diabetic *Ldlr*$^{-/-}$ mice, hepatic CREBH expression did not reduce hyperglycemia or alter body weight, brown adipose tissue (BAT) weight, or white adipose tissue (WAT) weight (Figure 2A and Supplemental Figure 5). The diabetic mice exhibited moderate increases in both plasma cholesterol and TG levels, which were prevented by hepatic CREBH expression (Figure 2, B and C). Analyses of the lipoprotein profiles are shown below (Figure 3, A and B). The similar increases in cholesterol and TGs in diabetic mice versus nondiabetic mice supported the proposal that the particles accumulating are remnants, which contain a more equal cholesterol-to-TG ratio than do large TG-rich chylomicrons and VLDL. The plasma TG levels in the nondiabetic mice were also significantly lower in the CREBH-overexpressing mice (Figure 2, B and C).

Analysis of plasma levels of apolipoproteins by targeted mass spectrometry revealed markedly elevated APOE in the diabetic mice (Figure 2D), consistent with previous evidence of impaired TRL clearance in diabetes (38). Hepatic expression of active CREBH reduced plasma APOE levels in both the nondiabetic and diabetic mice, indicating increased remnant clearance. Diabetes also increased levels of the APOC apolipoproteins (APOC1, APOC2, and APOC3), an effect not counteracted by CREBH. The increased plasma levels of APOC3 in the diabetic mice were consistent with our previous studies (21). CREBH modestly increased plasma levels of APOA4 and modestly reduced levels of APOB100, while APOA1 levels were unaffected (Figure 2D). Therefore, of the apolipoproteins analyzed, CREBH most strikingly reduced the elevated plasma APOE levels in diabetic mice. This reduction is in contrast to the increased hepatic *Apoe* mRNA

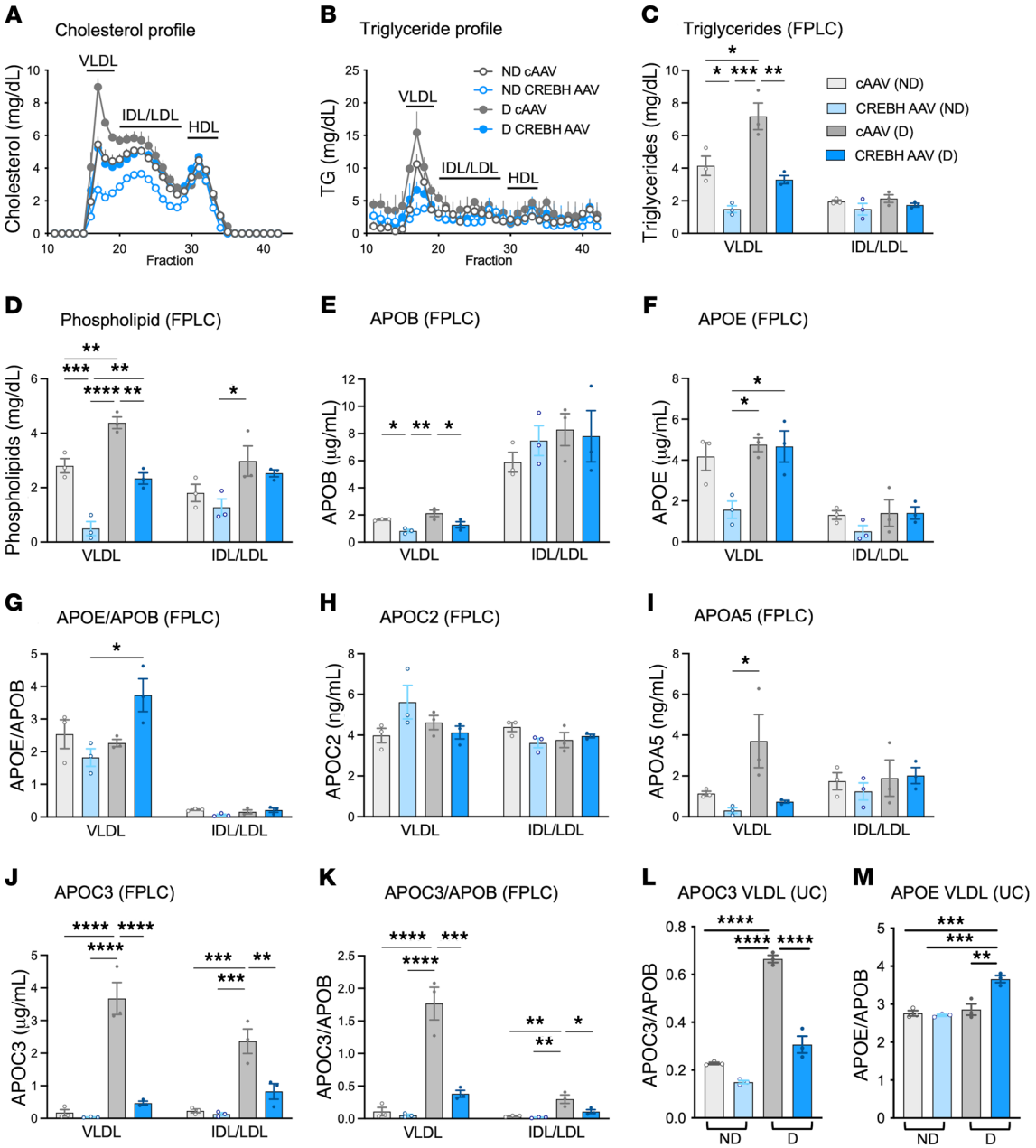

Figure 3. Hepatic CREBH activity results in APOE enrichment and APOC3 impoverishment of TRLs and remnants in diabetic mice. Plasma samples were separated by FPLC (pooled plasma of 2–3 mice/*n*, *n* = 3/group). Cholesterol (**A**) and TG (**B**) were measured in each fraction, generating lipoprotein profiles. (**C**–**K**) TGs, phospholipids, APOB, APOC3, APOC2, APOA5, and APOE were measured in the VLDL peak fraction (#17) and the IDL/LDL peak fraction (#22). Apolipoproteins were measured by ELISA. The relative levels of APOE and APOC3 in VLDL and IDL/LDL peak fractions were normalized to APOB (**G** and **K**), providing an estimate of APOE and APOC3 molecules/lipoprotein particle. (**L** and **M**) VLDL was isolated by ultracentrifugation (UC) and APOC3 and APOE were analyzed by ELISA and normalized to APOB (*n* = 3). Mean ± SD. **P* < 0.05; ***P* < 0.01; ****P* < 0.001; *****P* < 0.0001 by 2-way ANOVA followed by Tukey's multiple comparisons test. D, diabetic mice; ND, nondiabetic mice.

levels, suggesting that CREBH is increasing removal of APOE and its associated remnants from the circulation.

The apolipoprotein composition of lipoprotein particles determines metabolic fate. The elevated TG levels in diabetic mice have been explained by reduced hepatic clearance of TRLs (38) and reduced LPL expression in heart, skeletal muscle, and WAT, resulting in reduced TRL lipolysis (39). Conversely, CREBH deficiency has been described to increase plasma TGs through impairing LPL activity by reduced expression of its target genes APOC2 and APOA5 (LPL activators) and indirectly through increased levels of APOC3 (LPL inhibitor; ref. 2).

We therefore used size-exclusion chromatography–fast protein liquid chromatography (FPLC) and density ultracentrifugation to investigate the effects of diabetes and hepatic CREBH on the apolipoprotein composition of lipoprotein particles isolated in the VLDL, IDL, and LDL ranges. The FPLC lipoprotein profiles indicated that diabetic mice had higher cholesterol and TG levels, primarily in VLDL fractions and lipoproteins sized between

VLDL and LDL (likely IDL), with no increase in HDL (Figure 3, A and B). Note that the VLDL fractions contained chylomicron remnants, as there is no reliable method for differentiating VLDL from chylomicron remnants in mice. CREBH expression prevented the increase in VLDL and IDL with diabetes. CREBH also lowered cholesterol in the nondiabetic mice, primarily in VLDL but also in IDL and LDL.

We then measured TGs, phospholipids, APOC2, APOA5, APOC3, and APOB levels in the peak fractions of VLDL and IDL/LDL. As indicated by the TG lipoprotein profile (Figure 3B), VLDL TG levels were higher in the diabetic mice than in the nondiabetic mice, and CREBH reduced VLDL TG levels in both (Figure 3C). A similar pattern was observed for phospholipids (Figure 3D). Because VLDL APOB levels were similar in the diabetic and nondiabetic mice (Figure 3E) and because there is 1 APOB molecule per lipoprotein particle in APOB-containing lipoproteins, the increased levels of TGs and phospholipids indicated larger VLDL particles in diabetes, consistent with reduced lipolysis. On the other hand, hepatic CREBH expression markedly reduced APOB levels as well as TGs and phospholipids in the VLDL peak fraction, suggesting fewer VLDL/remnant particles through increased hepatic clearance (Figure 3, C–E).

The diabetic mice expressing hepatic CREBH had markedly higher levels of APOE in the VLDL peak fraction than the nondiabetic mice expressing CREBH (Figure 3F). This effect was still significant when normalized to APOB (Figure 3G). Conversely, levels of the CREBH targets APOC2 and APOA5 (which augment LPL activation) were not altered by CREBH, but APOA5 was increased by diabetes (Figure 3, H and I). Thus, the levels of these apolipoproteins were primarily regulated posttranscriptionally, we presume by their plasma clearance.

APOC3 levels were dramatically increased by diabetes, both in the VLDL and IDL/LDL peak fractions as compared with those of the nondiabetic mice (Figure 3J). Hepatic CREBH expression prevented this increased loading of APOC3 onto VLDL and IDL/LDL in the diabetic mice, indicating lower levels of remnants in the diabetic mice that expressed CREBH. In the IDL/LDL size range, APOC3 levels in plasma from diabetic mice were highest in fraction 22 (Supplemental Figure 6A), which eluted slightly before the main LDL peak, suggesting that these particles were smaller remnants or large LDL particles. This pattern was confirmed when APOC3 levels were normalized to APOB levels, either in VLDL and IDL/LDL peak fractions from FPLC (Figure 3K) or when lipoproteins in the VLDL density range were isolated by density ultracentrifugation (Figure 3L). Likewise, the pattern of APOE loading of VLDL (an increase in the diabetic mice expressing CREBH) was confirmed in VLDL isolated by density ultracentrifugation (Figure 3M).

The apolipoprotein composition, particle concentration, and function of HDL were also investigated. As shown in Supplemental Figure 6, B–D, diabetes increased levels of APOA4, APOC3, and APOE in HDL. The main effect of CREBH was to increase the APOA4 level in HDL in the nondiabetic mice. Neither diabetes nor CREBH affected total HDL particle concentrations as measured by calibrated ion mobility analysis, or HDL's cholesterol efflux capacity.

Together, these findings demonstrate that CREBH increases APOE loading and reduces APOC3 loading of TRLs and their remnants in diabetic mice. These compositional changes suggest that the particles are less atherogenic.

CREBH acts largely through an LPL-independent mechanism to lower remnants. We next investigated the mechanisms whereby diabetes and hepatic CREBH activity alter plasma TGs and cholesterol. While diabetes has been shown to increase TGs by suppressing LPL (39), CREBH is believed to lower plasma TGs by activating LPL (2). Total LPL activity can be analyzed in plasma after a heparin injection, which releases LPL from the glycosaminoglycans and GPIHBP1 on microvascular endothelial cells. Our analysis revealed that neither diabetes nor CREBH altered total post-heparin plasma LPL activity (Figure 4A). However, diabetes reduced LPL activity in BAT and CREBH had a small overall stimulatory effect, which was only seen in nondiabetic mice (Figure 4B). Neither diabetes nor CREBH altered LPL activity in heart, skeletal muscle, or WAT and did not consistently alter *Lpl* mRNA levels or mRNA levels of the LPL inhibitors *Angptl4* and *Angptl8* (Supplemental Figure 7, A–D). Moreover, CREBH slightly increased hepatic expression of *Angptl3*, another LPL inhibitor, rather than reduced it (Supplemental Figure 4A) and slightly reduced pre-heparin plasma lipase activity, which primarily reflects reduced hepatic lipase activity (Supplemental Figure 7E). Thus, we found no evidence of lipase activation by CREBH in diabetic mice. Plasma adiponectin levels were similar in all groups (Supplemental Figure 7F).

Because CREBH reduced APOC3 loading onto VLDL while diabetes increased APOC3/VLDL particles, we next investigated whether CREBH or diabetes could indirectly alter LPL activity by changing VLDL's composition. We used VLDL isolated by size-exclusion chromatography from the 4 groups of mice to investigate whether the different composition of VLDL would influence the activity of recombinant LPL. The results, which were normalized to APOB levels (VLDL particle number), showed that recombinant LPL activity was increased mainly by VLDL from CREBH-expressing nondiabetic mice (Supplemental Figure 7G). Together, these results indicate that CREBH does not increase total or tissue LPL activity in diabetic mice but that the altered composition of VLDL has the potential to increase LPL activity, at least when normalized to VLDL particle number in vitro. The in vivo relevance of this finding is uncertain, given that mice expressing CREBH have lower VLDL particle levels.

We therefore hypothesized that CREBH expression lowers plasma TG and cholesterol levels largely through an LPL-independent mechanism. To investigate this hypothesis, we used mice with inducible LPL deficiency ($iLpl^{-/-}$ mice). As expected, baseline TG levels were high in these mice as compared with floxed controls fed a high-fat diet (558 ± 73 mg/dL versus 103 ± 11 mg/dL; mean ± SEM; $n = 7$ and $n = 8$, respectively; $P = 0.0003$ by Mann-Whitney test). Hepatic CREBH expression reduced both TGs and cholesterol in the $iLpl^{-/-}$ mice (Figure 4C), presumably because of a reduction in VLDL. Importantly, these mice express endogenous LDLR, demonstrating that the effect of CREBH on plasma TGs and cholesterol are not unique to LDLR-deficient mice. These results confirm that CREBH lowers plasma TGs and cholesterol largely through an LPL-independent mechanism.

Hepatic CREBH requires APOE and LDL family receptors to lower circulating remnants. Remnants are cleared by the liver through

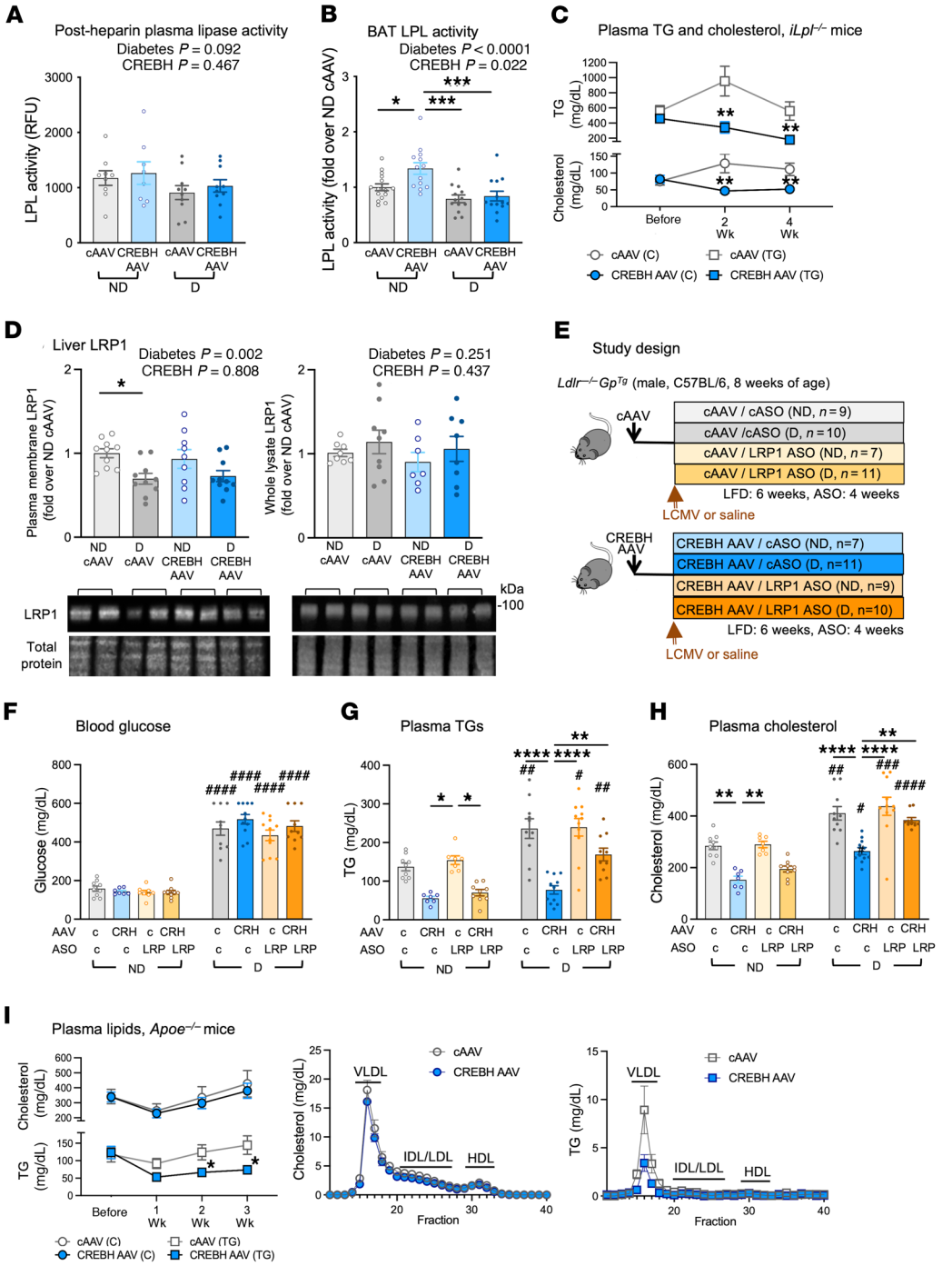

Figure 4. CREBH promotes lipid clearance through an APOE-dependent mechanism. After 3 weeks of diabetes, plasma was collected 5 minutes after heparin i.v. injection. (**A**) Heparin-releasable LPL activity was determined by subtracting pre-heparin plasma lipase activity in each mouse (n = 9 nondiabetic [ND] cAAV, n = 8 ND CREBH AAV, n = 10 diabetic [D] cAAV and D CREBH AAV). (**B**) LPL activity in brown adipose tissue (BAT) 4 weeks after diabetes induction (n = 14 ND cAAV; n = 13 ND CREBH AAV, D cAAV, and D CREBH AAV). (**C**) Plasma lipid levels at indicated times in mice with inducible LPL deficiency (*iLpl*$^{-/-}$) injected with CREBH AAV or cAAV (n = 7 cAAV, n = 9 CREBH AAV). (**D**) Diabetic and nondiabetic mice expressing CREBH were maintained for 4 weeks. Whole-liver lysate (n = 8 ND cAAV, n = 9 ND CREBH AAV, n = 7 D cAAV, n = 8 D CREBH AAV) and plasma membranes (n = 10 ND cAAV, ND CREBH AAV, and D CREBH AAV; n = 9 D cAAV) were used for LRP1 immunoblot. (**E**) *Ldlr*$^{-/-}$ mice were injected with CREBH AAV or cAAV (5×10^{10} GC) and LCMV injected 1 week later. Mice were treated with a liver-targeted GalNAc LRP1 antisense oligonucleotide (ASO) or control ASO (cASO) once a week for 4 weeks from the onset of diabetes. (**F**) Plasma glucose was measured 3 weeks after diabetes induction. CRH, CREBH. (**G** and **H**) Plasma TG and cholesterol were measured at week 2 after induction of diabetes (n values shown in **E**). (**I**) Plasma lipids were measured at the indicated times after cAAV or CREBH AAV injection in male *Apoe*$^{-/-}$ mice (n = 6). Plasma lipid profiles at week 3 (pooled plasma of 2 mice/n, n = 3/group). Mean ± SEM. $^{*}P < 0.05$; $^{**}P < 0.01$; $^{***}P < 0.001$; $^{****}P < 0.0001$ by 2-way ANOVA (overall effects shown above panels) followed by Tukey's multiple comparisons test or 2-tailed unpaired t test. $^{\#}P < 0.05$; $^{\#\#}P < 0.01$; $^{\#\#\#}P < 0.001$; $^{\#\#\#\#}P < 0.0001$ denote significance versus the corresponding nondiabetic group.

LDL family receptors, the primary of which is LRP1 in our mouse model. Insulin promotes translocation of hepatic LRP1 from intracellular vesicles to the plasma membrane, facilitating remnant clearance (44). We therefore first investigated whether diabetes reduces levels of plasma membrane LRP1. Total hepatic LRP1 protein levels as well as LRP1 levels in a hepatic fraction enriched with plasma membrane were measured by immunoblotting (Supplemental Figure 8A). As shown in Figure 4D, diabetes modestly reduced plasma membrane LRP1 levels without affecting total hepatic LRP1 levels. CREBH, on the other hand, had no effect on LRP1 protein levels. Therefore, the benefits of increased CREBH expression were unlikely to be due to changes in LRP1 protein levels or plasma membrane translocation.

Our findings showed that hepatic CREBH reduced APOC3 loading and increased APOE loading of TRLs in diabetes. As APOC3 prevents clearance of TRLs and their remnants through interfering with LDL family receptors (28), and APOE is a critical mediator of hepatic clearance through these receptors, including LRP1 (30), we next investigated whether CREBH might facilitate hepatic uptake of TRLs or their remnants partly through an LRP1-dependent pathway. To silence hepatic expression of LRP1, we used a liver-targeted GalNAc-conjugated antisense oligonucleotide (ASO) specific for LRP1 (Supplemental Figure 8B). LRP1 was silenced in livers from nondiabetic and diabetic mice with and without hepatic CREBH expression, as shown by the study design in Figure 4E. All the diabetic mice were hyperglycemic, regardless of treatment (Figure 4F), showing that any effects on lipids did not result from an altered diabetic status.

Two weeks after induction of diabetes, the diabetic mice had elevated plasma cholesterol and TG levels that were reduced by hepatic expression of active CREBH, as expected. However, CREBH's ability to lower plasma cholesterol and TG levels in the diabetic mice was reduced in the mice with silenced LRP1 (Figure 4, G and H). Similar results were obtained after 4 weeks of diabetes (Supplemental Figure 8C), but at this later time point, LRP1 silencing further exacerbated the effect of diabetes on lipids. The ability of CREBH to lower plasma cholesterol and TGs was significantly reduced by LRP1 ASO in the diabetic mice: 43.3% ± 3.8% reduction in cholesterol in the cASO-treated mice versus 20.5% ± 4.4% in the LRP1 ASO–treated mice ($P = 0.0002$, Mann-Whitney) and 64.0% ± 6.0% reduction in TGs in the cASO-treated mice versus 38.0% ± 11.1% in LRP1 ASO–treated mice ($P = 0.041$, Mann-Whitney).

To investigate the dependence on APOE for CREBH's lipid-lowering effects, we next injected *Apoe*$^{-/-}$ mice with cAAV and CREBH AAV. The CREBH AAV resulted in increased hepatic expression of CREBH target genes, as expected, demonstrating that CREBH was active in the *Apoe*$^{-/-}$ mice (Supplemental Figure 9). As shown in Figure 4I, hepatic expression of CREBH failed to lower VLDL and remnant cholesterol levels in *Apoe*$^{-/-}$ mice. However, CREBH lowered VLDL TG levels, suggesting improved lipolysis in the absence of APOE, but not increased remnant clearance from the circulation. It is possible that CREBH activates LPL to a relatively large extent in nondiabetic APOE-deficient mice, as APOE has been reported to inhibit LPL activity (45).

Together, these results demonstrate that CREBH lowers plasma remnants by boosting the hepatic APOE-mediated clearance pathway through LDL family receptors.

Hepatic expression of CREBH prevents atherosclerotic lesion progression in diabetic mice. By the end of the experiment described in Figure 1A, 4 weeks of diabetes had not increased the size of preexisting advanced atherosclerotic lesions in the aortic sinus, as expected from our previous studies (21). However, the diabetic mice with targeted hepatic CREBH expression had smaller lesions than the diabetic mice injected with the cAAV (Figure 5A). In preexisting advanced lesions, diabetes increases necrotic core expansion (21). Consistently, necrotic core size increased in the diabetic mice, while CREBH expression prevented this effect (Figure 5, B and C), phenocopying the effect of APOC3 ASO we observed previously (21). The effects of diabetes on lesion progression were also manifested as increased content of lesion macrophages and α-smooth muscle actin–positive (α-SMA$^+$) smooth muscle cells. These changes were absent in the diabetic mice expressing active CREBH (Supplemental Figure 10). The groups did not differ in collagen area.

Because remnants of TRLs are small enough to get trapped in the artery wall and are enriched in APOE (46), we next determined the apolipoprotein content of the sinus lesions. As shown in Figure 5D, lesions from the diabetic mice had more APOE immunoreactivity than those from the nondiabetic mice, and CREBH expression prevented this increase. We verified the specificity of the anti-APOE antibody in lesions collected from APOE-deficient mice (Figure 5F). The pattern of APOE immunoreactivity in lesions correlated well with the pattern of APOE levels in plasma (Figure 2D), likely reflecting slower clearance of remnants in the diabetic mice and therefore increased arterial trapping. A similar pattern was observed for APOC3 (Figure 5, E and G). However, the 2 groups showed similar APOB and APOA1 immunoreactivity, suggesting no overall effect on the trapping of APOB lipoproteins (mainly LDL) or HDL (Supplemental Figure 10).

Consistent with the larger necrotic core in lesions from the diabetic mice, cell death (detected as TUNEL-positive cells) was increased in the luminal lesion area of diabetic mice and was reduced by CREBH (Figure 5H). However, the overall numbers of lesion TUNEL-positive cells were not different between the groups. The increase in TUNEL-positive cells in the luminal lesion area in diabetes was not due to reduced efferocytosis (evaluated as TUNEL-positive, Mac-2–positive cells according to the method of Schrijvers et al.; ref. 47).

In some mouse models, diabetes causes monocytosis and neutrophilia, which can exacerbate atherosclerosis (48). We therefore determined whether CREBH could counteract those effects, potentially explaining the slower lesion progression. Diabetes did not induce monocytosis in this model, consistent with our previous studies (21), and there was no effect of CREBH. Furthermore, although diabetes associated with neutrophilia, hepatic CREBH expression had no effect (Supplemental Figure 11A). Systemic inflammation, measured as increased plasma IL-18 levels in the diabetic mice, was also not improved by CREBH (Supplemental Figure 11B). Hence, the protective effects of CREBH on lesion progression in the setting of diabetes do not seem to be explained by changes in the number of circulating monocytes or neutrophils or by suppressed systemic inflammation, measured as plasma IL-18.

However, peritoneal macrophages from the diabetic mice contained more cholesteryl esters than macrophages from the

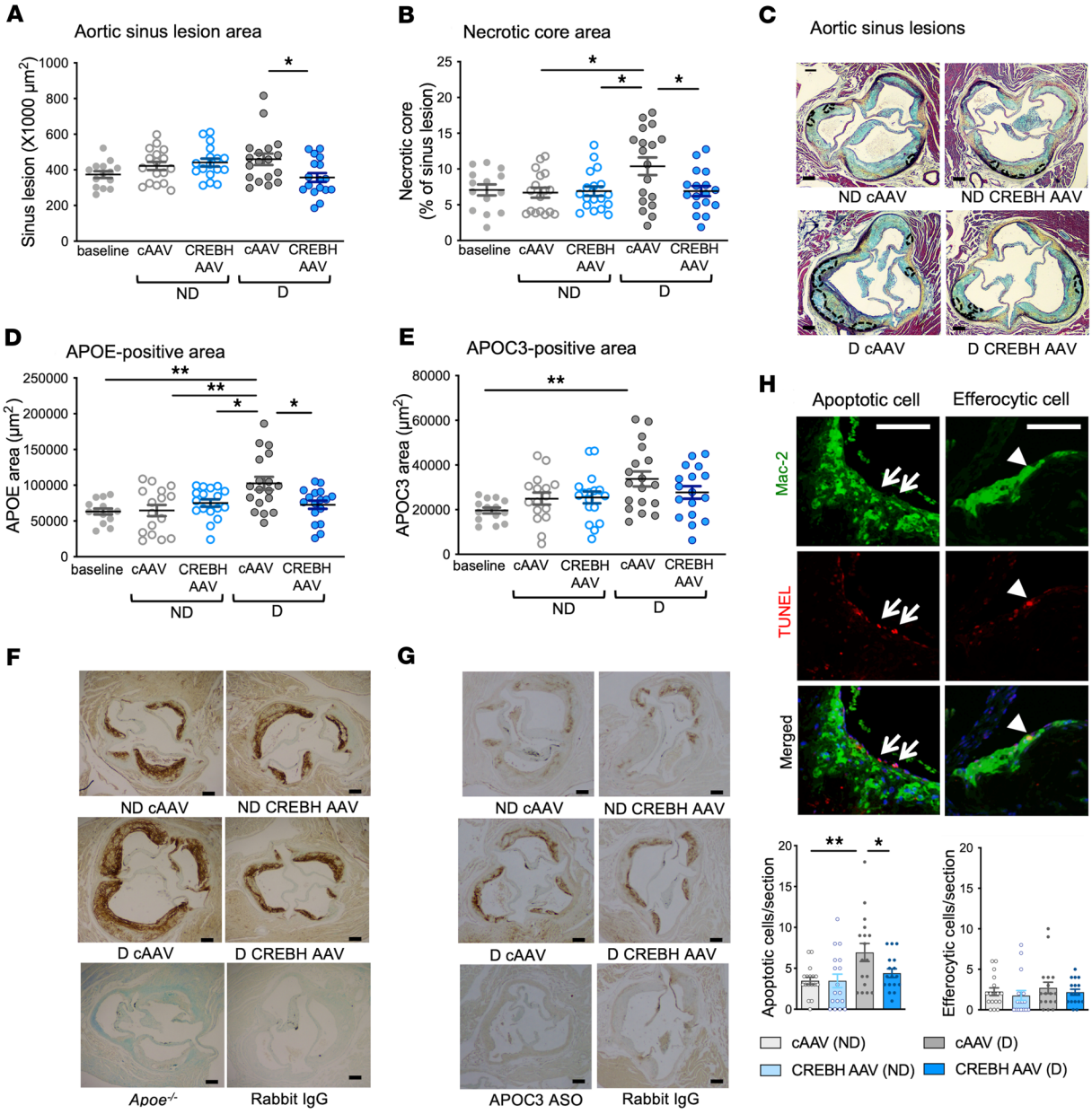

Figure 5. Hepatic expression of CREBH prevents the effects of diabetes on lesion necrotic core expansion and APOE accumulation. Diabetic (D) and nondiabetic (ND) mice with hepatic expression of active CREBH were generated as described in the Figure 1 legend. Atherosclerotic lesions in the aortic sinus were analyzed for cross-sectional lesion area (**A**) and necrotic core area as a percentage of lesion area (**B**) in sections stained using a Movat's pentachrome stain (**C**). In **C**, necrotic cores are marked by dashed lines. Immunohistochemistry was used to evaluate APOE-positive (**D** and **F**) and APOC3-positive (**E** and **G**) lesion areas. Rabbit IgG and lesions from *Apoe*$^{-/-}$ mice were used as negative controls for APOE immunohistochemistry. Rabbit IgG and lesions from mice treated with an APOC3 ASO21 were used as negative controls for APOC3 immunohistochemistry. (**H**) Cell death and efferocytosis were measured by TUNEL assay. Mean ± SEM. *$P < 0.05$; **$P < 0.01$ by 1-way ANOVA followed by Tukey's multiple comparisons test ($n = 14$ baseline, $n = 17$ ND cAAV, $n = 16$ ND CREBH AAV, $n = 18$ D cAAV, $n = 17$ D CREBH AAV). Scale bars: 100 μm.

nondiabetic mice, and this was prevented by hepatic CREBH expression (Supplemental Figure 11C). Furthermore, both circulating Ly6C^{hi} and Ly6C^{lo} monocytes from the diabetic mice exhibited increased side scatter by flow cytometry, a sign of lipid accumulation (49–51). CREBH prevented the increased side scatter in Ly6C^{lo} monocytes (Supplemental Figure 11D).

These findings suggested that the excess of remnants loaded with APOC3 in diabetic mice may be responsible for lesion expansion due to increased entrapment and accumulation of lipids in monocytes, macrophages, and lesions.

Human CREB3L3 loss-of-function or missense mutations associate with increased remnants and reduced APOE loading. Finally, we determined particle sizes and concentrations of the combined VLDL+IDL fraction (containing remnants of different sizes) isolated by ultracentrifugation from individuals with rare heterozygous loss-of-function or missense mutations in *CREB3L3*

and in age-matched controls with normal TG levels. We also analyzed the proteomes of the combined VLDL+IDL fractions. The mutations are described in Supplemental Table 1. Chylomicrons were removed prior to TRL isolation by density ultracentrifugation ($d < 1.019$ g/mL), and were not included in the analysis. The *CREB3L3* mutation group had an average age of 48.4 ± 4.5 years (7 males and 3 females) and the control group had an average age of 49.2 ± 3.7 years (6 males and 6 females; mean ± SEM). The subjects with loss-of-function and missense mutations in *CREB3L3* had higher plasma cholesterol and TG levels and lower HDL-cholesterol than the controls (Figure 6, A–C). Differential ion mobility analysis of VLDL+IDL particle concentrations (VLDL+IDL-P) and sizes in the combined VLDL+IDL fraction revealed increased accumulation of small remnants (25 nm diameter) in individuals with *CREB3L3* mutations (Figure 6D), which is consistent with an impaired hepatic clearance. There was also an increase in particles of larger sizes (28–50 nm; Figure 6E).

Targeted proteomic analyses of the combined VLDL+IDL fraction ($d < 1.019$ g/mL) demonstrated no differences in APOB100 or APOB48 content in samples normalized for total protein amount (Figure 6, F and G). Likewise, no differences were detected in the CREBH targets APOC2 and APOA4, or in APOC3 (Figure 6, H–J). However, there was a striking reduction in APOE in VLDL+IDL from individuals with *CREB3L3* mutations when measured either in isolation or normalized to APOB (Figure 6, K and L).

These results are consistent with the interpretation that CREBH acts primarily to slow clearance of remnants through an APOE-dependent pathway.

Discussion

Our study revealed a mechanism whereby CREBH reduces atherogenic lipids through enhanced hepatic clearance of TRL remnants. From mouse studies and the association of loss-of-function mutations of *CREB3L3* with hypertriglyceridemia in humans, CREBH was known to lower plasma TG levels. However, it was thought to act primarily by indirectly activating LPL through increased transcription of the LPL activators APOC2 and APOA5 (2). In contrast, we found that CREBH lowers both TGs and cholesterol largely through an LPL-independent pathway. Moreover, our results show that the hepatic remnant clearance pathway induced by CREBH is particularly important in diabetes — a state associated with impaired clearance of remnants and accelerated atherosclerosis. Our study therefore strengthens the evidence that diabetes exacerbates atherosclerosis by slowing clearance of remnant lipoproteins and suggests that increasing CREBH activity will overcome this defect.

How does CREBH restore the hepatic remnant clearance pathway in diabetes? We showed that CREBH increases hepatic expression of several targets involved in clearance of remnants and sterols from the body (most notably APOE, LRP1, VLDLR, ABCG5, and ABCG8). LRP1 binds to APOE in remnants to mediate their clearance. Individuals with remnant removal disease often are homozygous for the APOE2 isoform, which has reduced affinity for LRP1 and LDLR. Such individuals, when also affected by a second risk factor for dyslipidemia, have increased risk of atherosclerotic cardiovascular disease (17, 19). In addition to enhancing APOE loading of TRL remnants in diabetic mice, CREBH expression caused a dramatic loss of APOC3 on these particles. APOC3 is not a CREBH target gene (2) and accordingly, CREBH did not alter hepatic *Apoc3* mRNA levels in nondiabetic mice or the elevated *Apoc3* mRNA levels in diabetic mice. It is possible that the loss of APOC3 on TRL remnants in diabetic mice expressing CREBH is mediated by APOE displacement of APOC3 or by other changes in remnant properties. In general, there is a reciprocal relationship between APOC3 and APOE in TRLs. Thus, VLDL from APOC3-transgenic mice contain reduced levels of APOE as a result of the increased APOC3 loading of these particles (52). APOC3 has been shown to prevent hepatic TRL clearance through LDLR and LRP1 (28). Thus, CREBH likely increases hepatic clearance of remnants in part by enhancing hepatic APOE expression, markedly altering the APOE/APOC3 ratio of remnant lipoproteins, and the subsequent removal of these lipoproteins by APOE through LDL family receptors. This conclusion is strongly supported by our findings that while hepatic *Apoe* mRNA levels are increased, plasma levels of APOE decrease with greater CREBH expression. Moreover, silencing LRP1 by a liver-targeted ASO impaired CREBH's ability to lower TG and cholesterol levels in diabetic mice, CREBH failed to lower VLDL and remnant cholesterol in APOE-deficient mice, and individuals with loss-of-function mutations in CREBH had hyperlipidemia associated with increased levels of remnants and reduced levels of APOE in VLDL+IDL (Figure 6M). Although CREBH induced hepatic *Lrp1* mRNA levels, this effect did not produce a detectable increase in LRP1 protein in the liver plasma membrane fraction, suggesting that CREBH's effect on remnant removal is more likely mediated by reduced APOC3 and increased APOE. CREBH also increased expression of hepatic *Vldlr* mRNA, another receptor that binds and clears APOE-containing remnants (40). It is possible that the small residual remnant-lowering effect of CREBH in diabetic *Ldlr*$^{-/-}$ mice in which LRP1 had been silenced is mediated through APOE binding to VLDLR. In fact, we have previously shown that VLDLR overexpression prevents TRL accumulation and advanced atherosclerosis in our model of T1DM (53).

The exact mechanisms whereby CREBH increases hepatic *Apoe* mRNA levels need further study, given that *Apoe* is not a direct target of CREBH (2). In our studies, the increased hepatic *Apoe* mRNA expression might have resulted from CREBH's interaction with the nuclear receptor LXRα, a strong inducer of APOE (54). CREBH has been reported to coimmunoprecipitate with LXRα in liver samples (8). A mechanism dependent on physical interaction between CREBH and another nuclear receptor, PPARα, has recently been suggested to explain how CREBH can induce expression of genes without directly binding to their promoter regions (55). Moreover, posttranslational mechanisms could have contributed to the increased levels of APOE in TRLs and TRL remnants in diabetic mice expressing CREBH.

In addition, CREBH increased the expression of *Abcg5* and *Abcg8*, sterol transport proteins that mediate excretion of sterols to the bile. ABCG5, ABCG8, and APOE are targets of LXRs (54). One limitation of using LXR agonists as therapeutics for reducing plasma lipid levels and CVD is that LXR activation also increases hepatic lipogenesis (54). In our study, however, CREBH did not

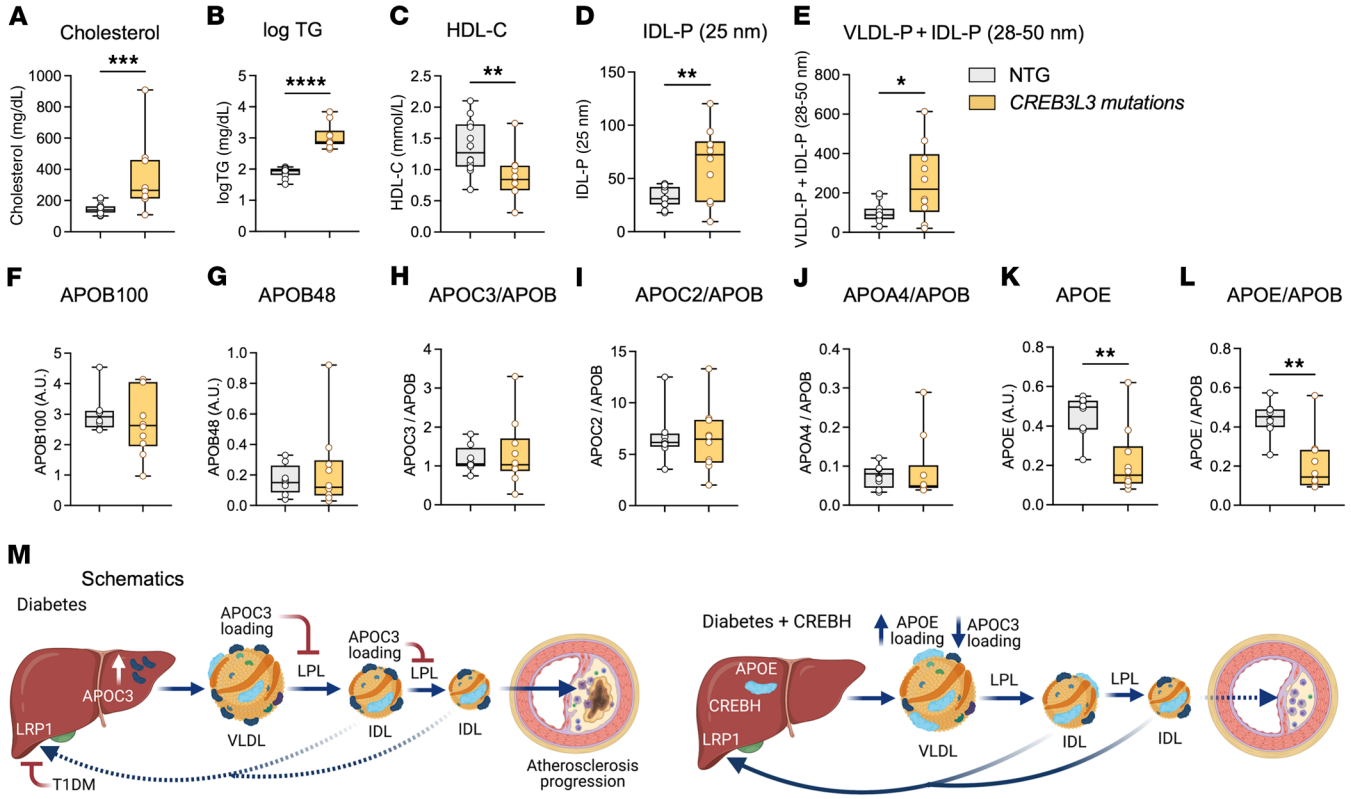

Figure 6. Human subjects with *CREB3L3* loss-of-function or missense mutations exhibit increased concentrations of small VLDL and IDL and reduced APOE in LDL/IDL. Age-matched human subjects with rare loss-of-function or missense mutations in *CREB3L3* and controls with normotriglyceridemia (NTG) were identified. (**A**) Plasma total cholesterol. (**B**) Plasma TG levels (logTG). (**C**) HDL-cholesterol levels. (**D**–**E**) VLDL and IDL were separated by density ultracentrifugation ($d > 1.019$ g/mL) after removal of chylomicrons. Total VLDL and IDL particle concentrations and sizes were measured by calibrated ion mobility analysis. (**F**–**L**) Apolipoproteins were quantified in the VLDL+IDL fraction ($d < 1.019$ g/mL) by targeted mass spectrometry. Data are shown as box-and-whisker plots, with boxes showing 25th to 75th percentile, horizontal lines showing medians, and whiskers showing minimum to maximum. $^*P < 0.05$, $^{**}P < 0.01$, $^{***}P < 0.001$, $^{****}P < 0.0001$ by unpaired, 2-tailed Mann-Whitney test ($n = 8$ for NTG and $n = 10$ for subjects with *CREB3L3* loss-of-function or missense mutations). (**M**) Schematic representation of the effects of diabetes and active CREBH on lipoproteins, apolipoproteins, and atherosclerosis. Poorly controlled T1DM results in increased hepatic production of APOC3, which leads to increased APOC3 loading of VLDL and remnants. The increased APOC3 load on VLDL mediates a reduced ability of LPL to hydrolyze VLDL and IDL. Diabetes also suppresses plasma membrane translocation of LRP1, further slowing clearance of remnants and leading to an increased accumulation of remnants in the artery wall, promoting lesion progression. Hepatic CREBH increases hepatic clearance of VLDL and IDL by enhancing the APOE loading of TRL remnants and depleting these particles of APOC3, thereby preventing the effects of diabetes on remnant accumulation and lesion progression (generated with BioRender.com).

appear to share the lipogenic actions of LXRs, because it did not induce hepatic *Fasn* levels or increase hepatic TG content.

Conversely, CREBH did not increase post-heparin plasma or tissue LPL activity in our study. Moreover, hepatic expression of CREBH markedly reduced levels of both plasma TGs and cholesterol in LPL-deficient mice, showing that it acts independently of LPL. Thus, although it is possible that our LPL activity measurements could have missed an effect of CREBH on the activity of LPL tethered to GPIHBP1 (14), CREBH is clearly able to lower TG and cholesterol levels even in the absence of LPL.

It was previously shown that CREBH's effect on plasma TG levels is not due to altered VLDL production (2, 32). Our data provide an explanation for what appears to be an effect on VLDL catabolism. One possibility we tested was that CREBH contributes to increased lipolysis of TRLs through increased expression of hepatic lipase, as its expression modestly induced *Lipc* mRNA. However, our data on the lack of CREBH stimulatory effects on pre-heparin plasma lipolysis do not support this interpretation. Furthermore, although CREBH both induced FGF21 expression and increased plasma levels of FGF21, its ability to clear TRL remnants and protect against atherosclerosis are most likely independent of FGF21, as recent studies have shown that CREBH suppresses atherosclerosis in *Fgf21*$^{-/-}$ mice (32). Moreover, FGF21 has been shown to reduce atherosclerosis by increasing adiponectin levels (56). CREBH did not alter plasma levels of adiponectin in our study, further casting doubt on a role for FGF21.

Our study also provides additional evidence that diabetes slows clearance of remnants and that this contributes to the enhanced progression of atherosclerosis. Our results point to 2 different mechanisms for slowing clearance (Figure 6M). First, diabetes associated with a modest increase in hepatic production of APOC3, which could partly explain the increased APOC3 loading of TRL remnants. Increased levels of APOC3 in TRLs are known to inhibit LPL's ability to hydrolyze TGs in these particles, slowing their conversion to remnants and subsequent hepatic clearance (14) and also to prevent TRL clearance through LDL

family receptors (28). Previous mouse models of T1DM have shown that diabetes impedes hepatic clearance of TRLs and inhibits LPL activity by reducing LPL expression in heart, skeletal muscle, and WAT (38, 39). Conversely, diabetes does not increase hepatic lipogenesis and VLDL production in a model of T1DM (39), which is consistent with the lack of increased lipogenic gene expression in the present study. In the current study, diabetes reduced tissue LPL activity in BAT, perhaps due to the dramatic APOC3 loading of TRLs. Secondly, we showed that diabetes associated with reduced plasma membrane levels of LRP1 in the liver, likely mediated by the relative insulin deficiency in diabetic mice. This finding is consistent with insulin's ability to increase translocation of LRP1 from internal membranes to the plasma membrane (44).

Importantly, we demonstrated that hepatic expression of active CREBH prevents diabetes from impairing remnant removal and promoting lesion progression. CREBH resulted in a dramatic loss of APOC3 loading of APOB-lipoproteins concomitant with an increase in APOE loading of TRLs, strongly indicating increased clearance of remnants. It is therefore likely that CREBH's protective effect on atherosclerosis in the setting of diabetes is due to reduced uptake and/or trapping of remnants in the artery wall. This is consistent with our observation that lesions from diabetic mice expressing CREBH were protected against increased levels of APOE and APOC3 and that myeloid cells were protected from lipid loading.

Finally, our study has clear human relevance because CREBH (*CREB3L3*) loss-of-function and missense mutations associate with severe hypertriglyceridemia (2, 5, 57). By analyzing a small cohort of individuals with rare *CREB3L3* loss-of-function mutations or missense mutations and controls, we demonstrated that subjects with *CREB3L3* mutations accumulate small remnant particles (25 nm diameter) that have reduced levels of APOE, suggesting impaired clearance of these particles. It should be noted, however, that very high TG levels saturate LPL-dependent lipolysis of TRLs in humans (58). It is therefore conceivable that the high TG levels in subjects with *CREB3L3* mutations are caused in part by reduced hepatic clearance of remnants and in part by saturation of LPL activity, resulting in increased levels of very large chylomicrons.

Could hepatic expression of CREBH be a therapeutic strategy for preventing CVD in diabetes? AAV8-based gene therapy strategies have yielded promising results in humans with hemophilia (59), and have been investigated in preclinical primate models for correcting dyslipidemia (60). It is therefore interesting to consider AAV8-mediated hepatic expression of the active portion of CREBH as a potential novel strategy for cardioprotection in states associated with impaired remnant removal and a residual CVD risk not preventable by LDL lowering.

Together, our results support the proposal that CREBH acts through a hitherto unknown APOE-dependent pathway to increase hepatic clearance of TRL remnants. They also provide more solid support for the hypothesis that impaired clearance of remnants plays an important role in atherosclerosis associated with T1DM.

Methods

Additional methods can be found in the supplemental material.

Mice. Male LDL receptor–deficient (*Ldlr*$^{-/-}$) *Gp*^{Tg} mice (8 weeks old at the beginning of a high-fat diet or a diabetogenic diet with added cholesterol) on the C57BL/6J background were used for the hepatic CREBH expression in diabetic mice and atherosclerosis study (described below). Male and female *Lpl*$^{fl/fl}$-actin-Cre mice (12–15 months old) on the C57BL/6J background were injected with tamoxifen to knock down LPL (*iLpl*$^{-/-}$). The mice were fed a standard chow diet. Age-matched control *Lpl*$^{fl/fl}$ littermates were injected with tamoxifen at the same time, and were fed a high-fat diet (Bio-Serv, S1850) to increase plasma lipids. CREBH AAV or cAAV (AAV8, 2×10^{11} GC/mouse, i.v.) was injected 2 weeks after the tamoxifen injection. Plasma TGs and cholesterol in individual mice were measured before the injection and 2 weeks and 4 weeks after. Another set of male *Ldlr*$^{-/-}$ *Gp*^{Tg} mice (8 weeks old) were injected with CREBH AAV or cAAV (AAV8, 2×10^{11} GC/mouse, i.v.). LCMV or saline was injected 1 week later. From the onset of diabetes the mice were treated with a liver-targeted GalNAc LRP1 ASO or control GalNAc ASO (described below) and maintained on a low-fat, semipurified diet (described in ref. 34) for 4 weeks. Male *Apoe*$^{-/-}$ mice on a C57BL/6J background (stock 002052), 8 weeks of age, were obtained from The Jackson Laboratory. They were fed the low-fat, semipurified diet 1 week prior to injection of CREBH AAV or cAAV and until termination of the experiment.

Production of liver-specific AAV-DJ/8 and AAV8 for expressing active CREBH. The pAAV2.1-TBG construct was obtained from the Vector Core at the Perelman School of Medicine University of Pennsylvania, and the mouse CREBH sequence (1–963 nt, 321 aa) or no sequence (control) was subcloned into the vector. HEK293D cells or HEK293 cells were transfected with the pAAV2.1-TBG constructs together with either a pAAV-DJ/8 capsid plasmid and pHelper (for AAV-DJ/8) or pDG capsid plasmid (for AAV8) in the presence of polyethylenimide. Two or 3 days later, all cells were harvested and cell pellets were digested by 4 repeated freeze-thaw cycles. The cell suspension was further treated with Benzonase (50 U/mL, 80108-806, EMD/VWR) for 30 minutes at 37°C and centrifuged. For purification of AAV-DJ/8, the virus-containing supernatant was applied to an iodixanol density gradient (15%, 25%, 40%, and 60%) and ultracentrifuged. The 40% layer was collected and purified by a HiTrap Heparin affinity column following by a HiTrap Desalt column. For purification of AAV8, the virus-containing lysate was purified by centrifugation on a sucrose cushion followed by isopycnic banding of the pelleted vector in a CsCl gradient for separation of full and empty capsids. The band containing full capsids was extracted from the gradient by needle aspiration and dialyzed in Hank's balanced salt solution, as described previously (61). Viral titers of the final preparation were determined by Southern blot, using sized DNA fragments as standards. AAV-DJ/8 and AAV8 resulted in similar effects in vivo.

Mouse model of T1DM-accelerated atherosclerosis. The T cell–induced *Ldlr*$^{-/-}$ *Gp*^{Tg} mouse model of T1DM-accelerated atherosclerosis has been described previously (34). These mice express the lymphocytic choriomeningitis virus (LCMV) glycoprotein (GP) under control of the insulin promoter. After the virus is injected, CD8^{+} T cells destroy β cells of the pancreas, inducing diabetes. To develop preexisting atherosclerosis, we first fed 8-week-old male *Ldlr*$^{-/-}$ *Gp*^{Tg} mice a high-fat, semipurified diet (40% calories from fat, 1.25% cholesterol; ref. 34) for 16 weeks. One week after they were switched to normal mouse chow (to reduce plasma cholesterol), the mice were injected with either control AAV (cAAV) or CREBH AAV (AAV-DJ/8, 5×10^{10} GC/mouse, i.v.). One week after the AAV injection, they were injected with LCMV to induce diabetes. Nondiabetic littermates were injected

with saline. On the same day and until the end of the study, the mice received a low-fat, semipurified diet (34) without added cholesterol (Figure 1A). Ten days after the LCMV injection, the onset of diabetes was documented (blood glucose > 250 mg/dL, as previously described; ref. 34). The diabetic mice received subcutaneous insulin pellets to provide baseline insulin (LinShin Canada Inc.), and were treated with insulin glargine (Lantus, Sanofi) to prevent weight loss and ketonuria as needed. Body weights were recorded daily.

At the end of the study, blood was collected and plasma was immediately isolated. Livers, intestines, and unilateral BAT and WAT (epididymal and inguinal) were collected, snap-frozen, and stored at −80°C prior to analysis. The lateral BAT and WAT (epididymal and inguinal) were kept on ice, and wet tissue weights were measured. Heart and aorta were collected and fixed in formalin. Macrophages from the peritoneal cavity were collected using ice-cold PBS plus 5 mM EDTA. The TG content of the liver was measured using a TG colorimetric assay kit (Cayman Chemical, 10010303).

Ldlr$^{-/-}$ *Gp*^{Tg} mice with and without diabetes were used for silencing of hepatic LRP1. Male mice (8 weeks old) were injected with either CREBH AAV or cAAV (2×10^{11} VG/mouse, i.v.). One week after the AAV injection, some mice were injected with LCMV to induce diabetes, and others were injected with saline as nondiabetic controls. At the onset of diabetes, the mice were injected with either an LRP1 GalNAc ASO or a control GalNAc ASO (5 mg/kg, i.p., weekly) produced by Ionis Pharmaceuticals (Figure 4E). At week 2, blood was collected from the saphenous vein for measurements of TGs and cholesterol. At the end of the study, after 4 weeks of diabetes, blood was collected and plasma was immediately isolated. Livers, intestines, BAT, WAT (epididymal and inguinal), heart, and skeletal muscle (hind limb) were collected, snap-frozen, and stored at −80°C until analysis.

Analysis of plasma and FPLC fractions. Blood glucose was measured in the saphenous vein blood by stick tests (OneTouch Ultra). As the glucometer does not go beyond 600 mg/dL, higher values were set to 600 mg/dL. Plasma cholesterol levels were determined by the Cholesterol E kit (Wako Diagnostics), and plasma TGs were determined by a colorimetric kit from Sigma-Aldrich. Plasma FGF21 and adiponectin were measured using ELISAs (Boster Biological Technology, EK1379 and ALPCO, 47-ADPMS-E01, respectively). To test for hepatotoxicity, we measured plasma levels of the liver enzyme alanine aminotransferase (ALT) with a kit from Sigma-Aldrich (MAK052-1KT). Plasma lipoprotein profiles were analyzed by size-exclusion FPLC, as described previously (34). Cholesterol and TGs were measured in each fraction. In the peak fractions for cholesterol of VLDL and LDL/IDL we measured APOC2, APOA5, APOE, and APOB using ELISAs from Aviva Systems Biology (OKEH05270), AVIVA (OKCD09560), MAB Tech Inc. (3752-1HP), and Abcam (ab230932), respectively. Plasma APOC3 and FPLC fractional APOC3 levels were measured using an APOC3 ELISA from Abcam (ab217777). To isolate VLDL fractions, we centrifuged pooled plasma at 3,220*g* for 10 minutes at 4°C and discarded the top lipid layer (chylomicrons). The rest of plasma was diluted 1:3 with PBS (d = 1.006 g/mL, total 500 μL) and then ultracentrifuged at 385,840*g* for 2 hours at 4°C. The top one-quarter volume (125 μL) was collected.

LPL activity measurements. Snap-frozen tissues (BAT, heart, hind limb skeletal muscle, and epididymal WAT) were weighed and either minced or homogenized with a Dounce homogenizer in ice-cold heparin buffer (5 U/mL heparin [H3149, Sigma-Aldrich], 2 mg/mL fatty acid–free BSA in PBS, 0.2 mg wet tissue/μL). Dispersed tissues were incubated for 1 hour in a 37°C shaker and then centrifuged at 5,400*g* for 10 minutes at 4°C. The supernatant was collected and used to assay lipase activity, according to a previously described method (62). The assay (100 μL) contained 25 μL of tissue supernatant in a reaction buffer (final 20 mM Tris-HCl, [pH 8.0], 0.15 M NaCl, 1.5% fatty acid–free BSA) in black 96-well plates. Immediately after adding 25 μL of a 4× mixture of EnzChek lipase substrate (final 0.8 μM, Invitrogen) and Zwittergent (final 0.0125%, Sigma-Aldrich), fluorescence at 482 nm/515 nm (excitation/emission) was measured for background values. After the plates were incubated for 30 minutes at room temperature, fluorescence was remeasured, and the background values were subtracted to obtain LPL activity. In some cases, recombinant human LPL (final 0.3 μg/mL, R&D Systems, 9888LL-100) and the FPLC VLDL fraction (25 μL) were preincubated for 30 minutes at room temperature before adding EnzChek substrate for LPL activity measurements. To measure plasma lipase activity, we collected blood from the saphenous vein before the mice received heparin. Post-heparin blood was collected 5 minutes after the heparin injection (300 U/kg heparin in PBS, i.v.). Both pre- and post-heparin plasma were used in the LPL activity assay, which contained 0.8 μM EnzChek lipase substrate, 0.0125% ZWITTERGENT in 20 mM Tris HCl (pH 8.0), 0.15 M NaCl, and 1.5% fatty acid–free BSA. Fluorescence values at 482 nm/515 nm were measured as described above. Post-heparin plasma LPL activity was obtained by subtracting pre-heparin from post-heparin fluorescence for each individual mouse.

Quantifying atherosclerosis. The aortic sinus was analyzed at 2 separate sites (90 μm apart), beginning when all 3 aortic valve leaflets appeared (63). Lesion size and necrotic core size at the 2 sites were averaged. Lesion macrophages were visualized by Mac-2 immunohistochemistry, using a monoclonal rat anti–mouse Mac-2 antibody (CL8942AP at 1 μg/mL; Cedarlane) (53). APOC3 immunohistochemistry was carried out with a rabbit polyclonal anti-APOC3 antibody generated by Ionis Pharmaceuticals (1:1000 dilution). Immunohistochemistry for APOB, APOE, and APOA1 was performed using a biotinylated goat anti-APOB antibody (R&D Systems, BAF3556; at 1:50), a rabbit monoclonal anti-APOE antibody (Abcam, ab183597; at 1:2000), and a goat anti-APOA1 antibody (Rockland Immunochemicals, 600-101-196, 1:4000), respectively. αSMA immunohistochemistry was performed using a rabbit anti-αSMA antibody (Abcam, ab5694; at 1:1000). Negative isotype controls (or serum controls) of the same concentrations or dilutions were used as controls (Supplemental Figure 10). Collagens were stained with Picrosirius red (Polysciences, Inc.), and the staining was observed under a polarized microscope. Collagen bundles, which reflected yellow and red, were quantified.

To detect apoptotic and efferocytic cells, we microwaved sinus sections for 1 minute in citrate buffer (pH 6.0), and treated them according to the manufacturer's protocol with a cell death detection reagent based on terminal deoxynucleotidyl transferase dUTP nick end labeling (TUNEL) (Boehringer Mannheim, 12156792910). The sections were then stained with anti–Mac-2 antibody followed by anti-rat secondary antibody conjugated with FITC. The sections were mounted in ProLong Gold Antifade Reagent with DAPI (Invitrogen). TUNEL and Mac-2 staining visualized using a fluorescence microscope was captured and quantified in Photoshop to evaluate apoptotic and efferocytic events.

Real-time PCR. Gene expression in liver, intestine, skeletal muscle, WAT, and BAT was quantified by real-time PCR. RNA isolation from liver, intestine, and BAT was performed using NucleoSpin RNA Plus kits (Macherey-Nagel), according to the manufacturer's protocols. Skeletal muscle RNA was isolated using the RNeasy Fibrous Tissue Kit (Qiagen, 74704). WAT was homogenized in QIAzol lysis reagent and an aqueous phase was separated after chloroform extraction. RNA in the aqueous phase was then isolated using RNeasy Mini Kits (Qiagen). Real-time PCR was performed using the SYBR Green 1 detection method (Thermo Fisher Scientific), as described previously (64). Cycle threshold (C_t) values were normalized to *Rn18s* and are presented as fold change versus control. Primer sequences are provided in Supplemental Table 2.

Analysis of liver plasma membrane LRP1 by immunoblotting. Whole-liver lysate and plasma membrane fractions were prepared with a plasma membrane protein isolation kit (Invent Biotechnologies, SM-005) containing protease inhibitor cocktail (Thermo Fisher Scientific, 1860932) and phosphatase inhibitor cocktail (Sigma-Aldrich, P0044). Protein samples were separated in SDS-PAGE gels and transferred to nitrocellulose membranes. Immunoblots for LPR1 and Na^+/K^+ ATPase were performed using a rabbit anti-LRP1 antibody (Invitrogen, MA5-31959; 1:2000 dilution), a rabbit anti–Na^+/K^+ ATPase antibody (Cell Signaling Technology, 3010S; 1:1000 dilution), and an IRDye 800CW anti-rabbit (LICOR) secondary antibody. Signal intensity of target proteins was normalized to Revert 700 Total Protein Stain (LICOR) or β-actin.

Liquid chromatography–electrospray ionization tandem mass spectrometric analysis of plasma, TRLs, and HDL-associated proteins. Liquid chromatography–electrospray ionization targeted tandem mass spectrometric (LC-ESI-MS/MS) analysis was used to determine selected proteins in mouse plasma, mouse HDL, and human VLDL+IDL as described previously (21) and in the supplemental material. HDL functional assays and analysis of HDL particle concentration were performed as described in the supplemental material.

Human subjects. Plasma samples from patients with *CREB3L3* loss-of-function or missense mutations and age- and sex-matched normotriglyceridemic subjects were selected from the Lipid Genetics Clinic at the London Health Sciences Centre, University Hospital. Clinical and demographic information for each patient were collected at the time of their first clinic visit. Fasting lipid profiles were measured according to clinical standards of care using the Cobas C502 Analyzer (Roche). Sequencing was performed on genomic DNA, as described previously (5). Patients with familial chylomicronemia syndrome, diagnosed by the presence of biallelic rare variants in canonical triglyceride metabolism genes (65) and remnant removal disease, were excluded.

Statistics. Group sizes were determined prior to the start of the study by power calculations. Littermate mice were randomized into different groups based on similar body weights. Differences in the number of mice/treatment group are due to the use of littermate controls from our colonies and to mice excluded by the following predetermined criteria: malocclusion, severe weight loss in poorly controlled diabetic mice, and failure of diabetes induction (LCMV-injected mice that never had blood glucose values above 250 mg/dL). All analyses were done in a masked fashion on coded samples. Statistical analyses were performed using GraphPad Prism 9.0.2. We used 2-tailed unpaired Student's *t* tests to compare differences between 2 groups when the data were normally distributed and when a sufficient number of data points per group allowed this. To compare 3 or more groups, we used either 1-way ANVOA or 2-way ANOVA followed by Tukey's or Sidak's post hoc tests, as indicated in each figure legend. D'Agostino-Pearson omnibus normality tests were performed to evaluate if the data were normally distributed. Data not normally distributed were analyzed by Mann-Whitney tests (for 2 group comparisons). A *P* value of less than 0.05 was considered statistically significant. All statistically significant comparisons are shown.

Study approval. All mouse experiments were performed in accordance with an approved University of Washington Institutional Animal Care and Use Committee protocol (protocol 3154-01) or an approved protocol at New York University (protocol 160907). In adherence to the Declaration of Helsinki, all patients provided written, informed consent for collection of personal data and DNA prior to inclusion in the study with approval from the Western University (London, ON, Canada) ethics review board (no. 07290E). All samples were deidentified and were analyzed in a blinded manner.

Author contributions

KEB designed and directed the study. IJG, JWH, and RAH provided additional direction. RAH provided plasma samples from subjects with *CREB3L3* mutations and controls. MSA and KEB wrote the manuscript. MSA, DB, JEK, FK, VK, SB, CT, NCF, and TV performed experiments and analyzed data. AEM provided advice and reagents. All authors reviewed the manuscript and provided final approval for submission.

Acknowledgments

This study was supported by NIH grants (R35HL150754 and P01HL151328 to KEB; P01HL151328 and R01HL45095 to IJG); a Career Development Award from the American Heart Association (20CDA35320109 to DB); a fellowship from the American Diabetes Association (number 9-18-CVD1-002 to VK); support from the National Lipid Association and N. Berrie Foundation (to DB); the Vector and Transgenic Mouse Core, Diabetes Research Center at University of Washington (NIH grant P30DK017047); and the University of Washington Nutrition and Obesity Research Center (NIH grant P30DK035816).

Address correspondence to: Karin Bornfeldt, University of Washington School of Medicine, Department of Medicine, Division of Metabolism, Endocrinology and Nutrition, 750 Republican Street, Seattle, Washington 98109, USA. Phone: 206.543.1681; Email: bornf@uw.edu.

1. Omori Y, et al. CREB-H: a novel mammalian transcription factor belonging to the CREB/ATF family and functioning via the box-B element with a liver-specific expression. *Nucleic Acids Res*. 2001;29(10):2154–2162.
2. Lee JH, et al. The transcription factor cyclic AMP-responsive element-binding protein H regulates triglyceride metabolism. *Nat Med*. 2011;17(7):812–815.
3. Cefalu AB, et al. Novel CREB3L3 nonsense mutation in a family with dominant hypertriglyceridemia. *Arterioscler Thromb Vasc Biol*. 2015;35(12):2694–2699.
4. Lee AH. The role of CREB-H transcription factor in triglyceride metabolism. *Curr Opin Lipidol*.

2012;23(2):141–146.
5. Dron JS, et al. Loss-of-function *CREB3L3* variants in patients with severe hypertriglyceridemia. *Arterioscler Thromb Vasc Biol*. 2020;40(8):1935–1941.
6. Nakagawa Y, Shimano H. CREBH regulates systemic glucose and lipid metabolism. *Int J Mol Sci*. 2018;19(5):E1396.
7. Nakagawa Y, et al. CREB3L3 controls fatty acid oxidation and ketogenesis in synergy with PPARα. *Sci Rep*. 2016;6:39182.
8. Zheng Z, et al. CREBH couples circadian clock with hepatic lipid metabolism. *Diabetes*. 2016;65(11):3369–3383.
9. Danno H, et al. The liver-enriched transcription factor CREBH is nutritionally regulated and activated by fatty acids and PPARalpha. *Biochem Biophys Res Commun*. 2010;391(2):1222–1227.
10. Khan HA, Margulies CE. The role of mammalian Creb3-like transcription factors in response to nutrients. *Front Genet*. 2019;10:591.
11. Ruppert PMM, et al. Transcriptional profiling of PPARα$^{-/-}$ and CREB3L3$^{-/-}$ livers reveals disparate regulation of hepatoproliferative and metabolic functions of PPARα. *BMC Genomics*. 2019;20(1):199.
12. Nakagawa Y, et al. Hepatic CREB3L3 controls whole-body energy homeostasis and improves obesity and diabetes. *Endocrinology*. 2014;155(12):4706–4719.
13. Basu D, Bornfeldt KE. Hypertriglyceridemia and atherosclerosis: using human research to guide mechanistic studies in animal models. *Front Endocrinol (Lausanne)*. 2020;11:504.
14. Larsson M, et al. Apolipoprotein C-III inhibits triglyceride hydrolysis by GPIHBP1-bound LPL. *J Lipid Res*. 2017;58(9):1893–1902.
15. Sacks FM. The crucial roles of apolipoproteins E and C-III in apoB lipoprotein metabolism in normolipidemia and hypertriglyceridemia. *Curr Opin Lipidol*. 2015;26(1):56–63.
16. Chait A, et al. Remnants of the triglyceride-rich lipoproteins, diabetes, and cardiovascular disease. *Diabetes*. 2020;69(4):508–516.
17. Chait A, et al. Type-III Hyperlipoproteinaemia ("remnant removal disease"). Insight into the pathogenetic mechanism. *Lancet*. 1977;1(8023):1176–1178.
18. Morganroth J, et al. The biochemical, clinical, and genetic features of type III hyperlipoproteinemia. *Ann Intern Med*. 1975;82(2):158–174.
19. Koopal C, et al. Vascular risk factors, vascular disease, lipids and lipid targets in patients with familial dysbetalipoproteinemia: a European cross-sectional study. *Atherosclerosis*. 2015;240(1):90–97.
20. Josefs T, et al. Atherosclerosis regression and cholesterol efflux in hypertriglyceridemic Mice. *Circ Res*. 2021;128(6):690–705.
21. Kanter JE, et al. Increased apolipoprotein C3 drives cardiovascular risk in type 1 diabetes. *J Clin Invest*. 2019;129(10):4165–4179.
22. Basu A, et al. Serum apolipoproteins and apolipoprotein-defined lipoprotein subclasses: a hypothesis-generating prospective study of cardiovascular events in T1D. *J Lipid Res*. 2019;60(8):1432–1439.
23. Buckner T, et al. Association of apolipoprotein C3 with insulin resistance and coronary artery calcium in patients with type 1 diabetes. *J Clin Lipidol*. 2021;15(1):235–242.
24. Reyes-Soffer G, et al. Effects of APOC3 heterozygous deficiency on plasma lipid and lipoprotein metabolism. *Arterioscler Thromb Vasc Biol*. 2019;39(1):63–72.
25. Ramms B, et al. ApoC-III ASO promotes tissue LPL activity in the absence of apoE-mediated TRL clearance. *J Lipid Res*. 2019;60(8):1379–1395.
26. Stalenhoef AF, et al. Metabolism of apolipoproteins B-48 and B-100 of triglyceride-rich lipoproteins in normal and lipoprotein lipase-deficient humans. *Proc Natl Acad Sci U S A*. 1984;81(6):1839–1843.
27. Noel SP, et al. An in vitro model for the catabolism of rat chylomicrons. *Biochem Biophys Res Commun*. 1975;63(3):764–772.
28. Gordts PL, et al. ApoC-III inhibits clearance of triglyceride-rich lipoproteins through LDL family receptors. *J Clin Invest*. 2016;126(8):2855–2866.
29. Gaudet D, et al. Targeting APOC3 in the familial chylomicronemia syndrome. *N Engl J Med*. 2014;371(23):2200–2206.
30. Kowal RC, et al. Opposing effects of apolipoproteins E and C on lipoprotein binding to low density lipoprotein receptor-related protein. *J Biol Chem*. 1990;265(18):10771–10779.
31. Zhang K, et al. Endoplasmic reticulum stress activates cleavage of CREBH to induce a systemic inflammatory response. *Cell*. 2006;124(3):587–599.
32. Nakagawa Y, et al. Enterohepatic transcription factor CREB3L3 protects atherosclerosis via SREBP competitive inhibition. *Cell Mol Gastroenterol Hepatol*. 2020;11(4):949–971.
33. Satoh A, et al. CREBH improves diet-induced obesity, insulin resistance, and metabolic disturbances by FGF21-dependent and FGF21-independent mechanisms. *iScience*. 2020;23(3):100930.
34. Renard CB, et al. Diabetes and diabetes-associated lipid abnormalities have distinct effects on initiation and progression of atherosclerotic lesions. *J Clin Invest*. 2004;114(5):659–668.
35. Chen SJ, et al. Biodistribution of AAV8 vectors expressing human low-density lipoprotein receptor in a mouse model of homozygous familial hypercholesterolemia. *Hum Gene Ther Clin Dev*. 2013;24(4):154–160.
36. Xu X, et al. Transcriptional regulation of apolipoprotein A-IV by the transcription factor CREBH. *J Lipid Res*. 2014;55(5):850–859.
37. Park JG, et al. Loss of transcription factor CREBH accelerates diet-induced atherosclerosis in Ldlr$^{-/-}$ mice. *Arterioscler Thromb Vasc Biol*. 2016;36(9):1772–1781.
38. Goldberg IJ, et al. Decreased lipoprotein clearance is responsible for increased cholesterol in LDL receptor knockout mice with streptozotocin-induced diabetes. *Diabetes*. 2008;57(6):1674–1682.
39. Willecke F, et al. Lipolysis, and not hepatic lipogenesis, is the primary modulator of triglyceride levels in streptozotocin-induced diabetic mice. *Arterioscler Thromb Vasc Biol*. 2015;35(1):102–110.
40. Takahashi S, et al. The very low density lipoprotein (VLDL) receptor — a peripheral lipoprotein receptor for remnant lipoproteins into fatty acid active tissues. *Mol Cell Biochem*. 2003;248(1–2):121–127.
41. Connelly PW, Hegele RA. Hepatic lipase deficiency. *Crit Rev Clin Lab Sci*. 1998;35(6):547–572.
42. Patel SB, et al. ABCG5 and ABCG8: more than a defense against xenosterols. *J Lipid Res*. 2018;59(7):1103–1113.
43. Gordts P, Esko JD. The heparan sulfate proteoglycan grip on hyperlipidemia and atherosclerosis. *Matrix Biol*. 2018;71–72:262–282.
44. Laatsch A, et al. Insulin stimulates hepatic low density lipoprotein receptor-related protein 1 (LRP1) to increase postprandial lipoprotein clearance. *Atherosclerosis*. 2009;204(1):105–111.
45. Rensen PC, van Berkel TJ. Apolipoprotein E effectively inhibits lipoprotein lipase-mediated lipolysis of chylomicron-like triglyceride-rich lipid emulsions in vitro and in vivo. *J Biol Chem*. 1996;271(25):14791–14799.
46. Boren J, et al. Low-density lipoproteins cause atherosclerotic cardiovascular disease: pathophysiological, genetic, and therapeutic insights: a consensus statement from the European Atherosclerosis Society Consensus Panel. *Eur Heart J*. 2020;41(24):2313–2330.
47. Schrijvers DM, et al. Phagocytosis of apoptotic cells by macrophages is impaired in atherosclerosis. *Arterioscler Thromb Vasc Biol*. 2005;25(6):1256–1261.
48. Nagareddy PR, et al. Hyperglycemia promotes myelopoiesis and impairs the resolution of atherosclerosis. *Cell Metab*. 2013;17(5):695–708.
49. Jackson WD, et al. Very-low and low-density lipoproteins induce neutral lipid accumulation and impair migration in monocyte subsets. *Sci Rep*. 2016;6:20038.
50. Potteaux S, et al. Suppressed monocyte recruitment drives macrophage removal from atherosclerotic plaques of Apoe$^{-/-}$ mice during disease regression. *J Clin Invest*. 2011;121(5):2025–2036.
51. Xu L, et al. Foamy monocytes form early and contribute to nascent atherosclerosis in mice with hypercholesterolemia. *Arterioscler Thromb Vasc Biol*. 2015;35(8):1787–1797.
52. Aalto-Setala K, et al. Mechanism of hypertriglyceridemia in human apolipoprotein (apo) CIII transgenic mice. Diminished very low density lipoprotein fractional catabolic rate associated with increased apo CIII and reduced apo E on the particles. *J Clin Invest*. 1992;90(5):1889–1900.
53. Johansson F, et al. Type 1 diabetes promotes disruption of advanced atherosclerotic lesions in LDL receptor-deficient mice. *Proc Natl Acad Sci U S A*. 2008;105(6):2082–2087.
54. Wang B, Tontonoz P. Liver X receptors in lipid signalling and membrane homeostasis. *Nat Rev Endocrinol*. 2018;14(8):452–463.
55. Kim H, et al. Regulation of hepatic circadian metabolism by the E3 ubiquitin ligase HRD1-controlled CREBH/PPARα transcriptional program. *Mol Metab*. 2021;49:101192.
56. Lin Z, et al. Fibroblast growth factor 21 prevents atherosclerosis by suppression of hepatic sterol regulatory element-binding protein-2 and induction of adiponectin in mice. *Circulation*. 2015;131(21):1861–1871.
57. D'Erasmo L, et al. Spectrum of mutations and long-term clinical outcomes in genetic chylomi-

cronemia syndromes. *Arterioscler Thromb Vasc Biol*. 2019;39(12):2531–2541.
58. Brunzell JD, et al. Evidence for a common, saturable, triglyceride removal mechanism for chylomicrons and very low density lipoproteins in man. *J Clin Invest*. 1973;52(7):1578–1585.
59. Nathwani AC, et al. Long-term safety and efficacy of factor IX gene therapy in hemophilia B. *N Engl J Med*. 2014;371(21):1994–2004.
60. Greig JA, et al. Non-clinical study examining AAV8.TBG.hLDLR vector-associated toxicity in chow-fed wild-type and LDLR$^{+/-}$ rhesus macaques. *Hum Gene Ther Clin Dev*. 2017;28(1):39–50.
61. Halbert CL, et al. AAV6 vector production and purification for muscle gene therapy. *Methods Mol Biol*. 2018;1687:257–266.
62. Basu D, et al. Determination of lipoprotein lipase activity using a novel fluorescent lipase assay. *J Lipid Res*. 2011;52(4):826–832.
63. Daugherty A, et al. Recommendation on design, execution, and reporting of animal atherosclerosis studies: a scientific statement from the American Heart Association. *Arterioscler Thromb Vasc Biol*. 2017;37(9):e131–e157.
64. Kanter JE, et al. Diabetes promotes an inflammatory macrophage phenotype and atherosclerosis through acyl-CoA synthetase 1. *Proc Natl Acad Sci U S A*. 2012;109(12):E715–E724.
65. Dron JS, et al. Severe hypertriglyceridemia is primarily polygenic. *J Clin Lipidol*. 2019;13(1):80–88.